We are IntechOpen,
the world's leading publisher of
Open Access books
Built by scientists, for scientists

6,900
Open access books available

186,000
International authors and editors

200M
Downloads

Our authors are among the

154
Countries delivered to

TOP 1%
most cited scientists

12.2%
Contributors from top 500 universities

CLARIVATE ANALYTICS
BOOK CITATION INDEX
INDEXED

WEB OF SCIENCE™

Selection of our books indexed in the Book Citation Index
in Web of Science™ Core Collection (BKCI)

Interested in publishing with us?
Contact book.department@intechopen.com

Metallic Glass Matrix Composites

Wei Guo

Additional information is available at the end of the chapter

http://dx.doi.org/10.5772/intechopen.76526

Abstract

In this chapter, we will firstly introduce the metallic glass and its deformation characteristics briefly. Then we will focus on the fabrication and mechanical properties of metallic glass matrix composites, including ex-situ particle/fiber reinforced, in-situ precipitated phase reinforced and etc. The alloy systems will cover from Zr-based, Ti-based to Mg-based and etc. We will also introduce the latest research on both new reinforcing phases and fabrication processes, including porous particles, shape memory phases, novel dealloying in metallic melt method, selective phase leaching method and so on. The microstructures, mechanical properties of each kind of composites, as well as the optimization methods, will be discussed in detail.

Keywords: metallic glass matrix composite, mechanical property, plasticity, fabrication process, shear band

1. Introduction

1.1. What is metallic glass?

The metallic glass or bulk metallic glass (BMG) is the alloy without crystals, or so-called non-crystalline alloys. In BMGs, the microstructure is so-called amorphous state, referring to the long-range disordered structures between atoms inside a material. The amorphous materials can be produced by non-crystalized cooling from melting state or vapor deposition, mechanical alloying methods, etc. To date, the amorphous materials occupy a large proportion in nature materials, from conventional oxide glass to amorphous semi-conductor, then to amorphous metals or bulk metallic glasses. The amorphous materials have been very important engineering materials to support the modern economy, as well as economic and social developments. Besides the daily-used glassy materials, in high-tech fields, amorphous materials

have been also applied a lot to optical communication, laser technology, new solar battery, power transmission materials and so on.

Unlike the conventional oxide glasses, the amorphous alloys or metallic glasses possess metallic bond between atoms instead of covalent bond. Thus, the characteristics related with metals are maintained, such as opacity, good toughness, etc. We can say the amorphous structure is faultless for the lack of dislocations or grain boundaries. We can also say the amorphous structure or random-arranged structure is full of defects because you can find no periodicity in it.

Even though both amorphous alloys and bulk metallic glasses are noncrystalline materials, which are obtained from rapid cooling from liquid state, hindering the crystallization kinetics [1]. The high rate of heat transfer required to prevent crystallization often limits these noncrystalline materials to thin samples or ribbon-shaped samples. These noncrystalline materials are called amorphous alloys. Recently, bulk metallic glasses with slower nucleation kinetics in undercooled liquids have been processed by conventional casting at cooling rate of 10^{-1}–10^{-2} K/s [2–6]. The critical size can be larger than 1 mm rods; these "bulk" noncrystalline alloys are called bulk metallic glasses. **Figure 1** illustrates the conditions for processing both the more recently developed bulk amorphous alloys as well as traditional metallic glass alloys developed before 1990 [4]. The plot correlating critical cooling rate and maximum sample thickness as a function of the reduced glass transition temperature (T_g/T_m) shows a clear tendency for the glass-forming ability to increase with increasing T_g/T_m, as such these alloys have lower critical cooling rates and larger possible bulk cross-sectional dimensions.
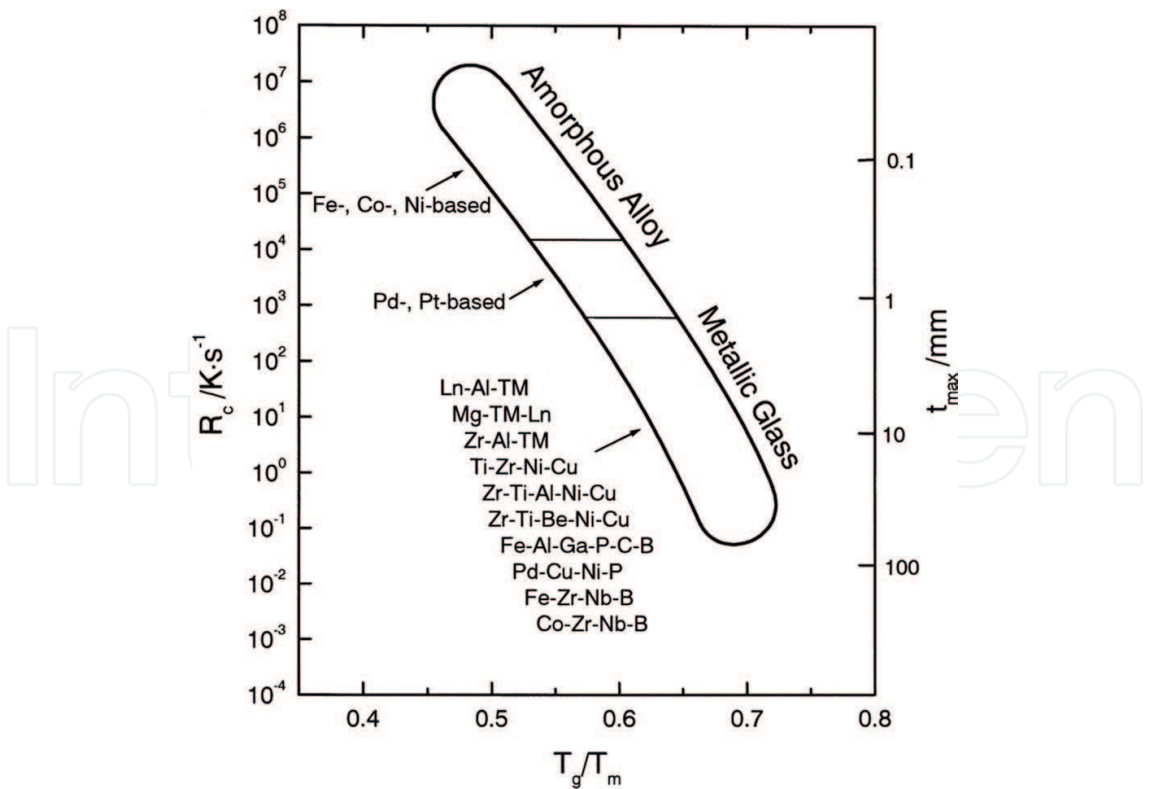

Figure 1. Plot correlating critical cooling rate (R_c), maximum sample thickness (t_{max}), and reduced glass transition temperature (T_g/T_m) for bulk metallic alloys illustrating conditions for processing both the more recently developed bulk amorphous alloys as well as ordinary amorphous alloys developed before 1990 [4].

The criteria [7–10] for slow crystallization kinetics, a stabilized supercooled liquid and high glass-forming ability, resulting in the formation of bulk metallic glasses, have been shown to include:

1. Multi-component alloys of increased complexity and size of crystal unit cells such that the energetic advantage of an ordered structure is reduced by increasing the configurational entropy of the supercooled liquid phases.

2. Atomic radius mismatch between elements, which leads to higher packing density and smaller free volume, requiring a greater volume increase for crystallization, as well as limiting the solubility of these atoms in crystalline states.

3. Negative heat of mixing between the elements, which increases the energy barrier at the solid–liquid interface and accelerates atomic diffusivity, thus slowing local atomic rearrangements and crystal nucleation rate, thereby extending the supercooled liquid temperature.

4. Alloy composition close to deep eutectic, which forms a liquid stable at low temperatures that can freeze into the glassy state.

1.2. Why study metallic glass?

The research and developments of BMGs indicate that compared with traditional crystalline materials, BMGs have an advantage in usability. The main points are as follows:

1. Better mechanical properties such as high yielding strength, large elastic strain limit, mainly perfect elasticity before yielding, mainly perfect plasticity after yielding, no work hardening, high fatigue resistance and high abrasive resistance. With the developments of BMGs, the ultimate strength of metallic materials is renewed again and again. The strength of Mg-based BMGs has increased from 600 to 800 MPa [11]. The strength of Cu-based BMGs is over 2000 MPa [12]. Especially for Co-Fe-Ta-B alloy, the strength is over 5000 MPa [12], which sets up a record in natural world.

2. Good processability. Near glass transition temperature (T_g), the elongation of La-Al-Ni BMGs can be 15,000% [13]. Other BMGs also show super-plasticity to varying degrees, thus according to different application, BMGs can be manufactured into micro- or nano-level by machining deformation.

3. Better corrosion resistance against many kinds of medium. The corrosion resistance of Fe-Cr-Mo-B-P BMGs is 10,000 times higher than conventional stainless steel and can be used in much severed environments [14].

4. Good physical properties such as soft and hard magnetism, unique expansive quantity. For example, the saturation magnetization of Fe-based amorphous alloys can be over 1.5 T and coercivity is lower than 1 A/m^2 [15]. When some BMGs are annealed to form nanocrystalline alloys, better soft or hard magnetism can be obtained, which are considered as excellent substitute for conventional materials.

For the better physical, chemical, mechanical properties and precision shaping abilities of BMGs than conventional materials, BMGs have shown important application value in aerospace device, precision machine, information technology and so on. The researches of BMGs have attracted a lot of attentions from physical, chemical and material scientists.

1.3. Room-temperature brittleness of metallic glass

Because of the metallic bonding in amorphous alloys, strain can be accommodated at the atomic level through changes in neighborhood; atomic bonds can be broken and reformed at the atomic scale. However, unlike crystalline metals and alloys, metallic glasses do not exhibit long-range translational symmetry. Thus, the deformation mechanisms such as dislocations, which allow changes in atomic neighborhood at low energies or stresses, do not exist in metallic glasses. The local rearrangement of atoms in metallic glasses is a relatively high-energy or high-stress process. The exact nature of local atomic motion in deforming metallic glasses is not fully understood, although there is general consensus that the fundamental unit must be a local rearrangement of atoms accommodating the shear strain. An example of such a local rearrangement is depicted in the two-dimensional schematic of **Figure 2a**, originally proposed by Argon and Kuo [16] on the basis of an atomic-analog bubble-raft model, called a "shear transformation zone" (STZ) [17–20]. The STZ is essentially a local cluster of atoms that undergoes an inelastic shear distortion from one relatively low energy configuration to a second such configuration, crossing an activated configuration of higher energy and volume. The STZs are common to deformation of all amorphous metals, although details of the structure, size and energy scales of STZs may vary from one glass to the other. In a metallic glass body experiencing uniform stress, the STZ that is activated first is selected from among many potential sites on the basis of energetics, which vary with the local atomic arrangements [21–23]. The continued propagation of the applied shear strain occurs when one STZ creates a localized distortion of the surrounding material, which triggers the formation of large planar bands of STZs along the maximum shear stress plane, or so-called "shear bands", as shown in **Figure 2b**. For most BMGs, the deformation occurs in homogeneous through plastic strains
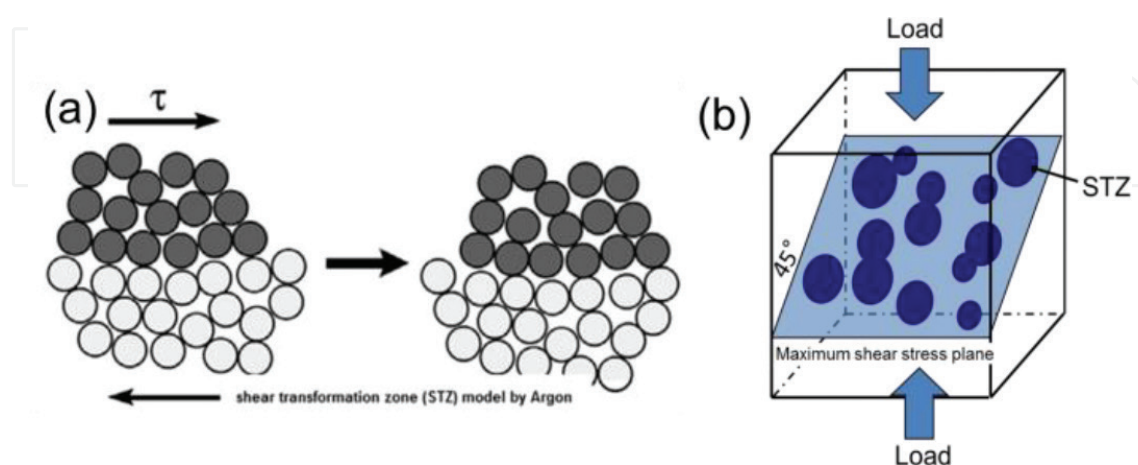

Figure 2. Schematic illustrating of (a) "shear transformation zone" in which strain accommodation occurs through localized cluster of atoms undergoing intense distortion and (b) shear band formation along maximum shear stress plane.

concentrated in localized shear bands at room temperature. Once a shear band initiates, the propagation of it can be very fast (~1000 m/s), thus, the BMGs fracture catastrophically after elastic deformation. Therefore, the room-temperature brittleness, especially under the uni-axial compression or tension, has been one fatal problem for the wide application of BMGs.

1.4. How to overcome the problem?

To date, there are several ways that have been developed to improve the room-temperature plasticity of BMGs, including intruding a secondary phase to develop a composite micro-structure, surface coating, composition adjustment to induce intrinsic heterogeneity, severe plastic deformation such as shot peening and high pressure torsion [24–27]. Although intro-ducing a secondary phase to make a composite structure seems to be most primal methods, it is reported that composite structure is one of the most efficient method and very easy to real-ize. Furthermore, there are many combinations of amorphous matrix and reinforcing phases, giving an infinite possibility to improve the mechanical properties of BMGs.

For now, there are mainly two ways to introduce the secondary phases, ex-situ direct adding and in-situ precipitation. For ex-situ method, the various combinations of secondary particle or fiber and the amorphous matrix makes the fabrication process easier to design. But the interface bonding between the secondary phase and the matrix is not strong because of the formation of surface oxide layers, which degrades the mechanical properties of them. For in-situ method, even though the interface bonding is stronger than those ex-situ composites because the secondary phases are intrinsically formed in the melt during cooling, but the fab-rication process is very difficult to design. Furthermore, for ex-situ method, the size and vol-ume fraction of secondary phases can be easily controlled by using various sized particles or fibers with various amounts when adding. However, for in-situ method, it is difficult to opti-mize the microstructures because the optimization process is related with the composition adjustment. Hereafter, we will introduce the researches on both ex-situ and in-situ BMGMCs, including their composite structure and mechanical properties.

2. Ex-situ BMGMCs

The selection of ex-situ secondary phases includes fibers, particles, pores and porous par-ticles. Hereafter, we will introduce the microstructures and mechanical properties of each kind of ex-situ BMGMCs.

2.1. Fiber-reinforced BMGMCs

The fiber-reinforced BMGMCs mainly focus on tungsten fiber, steel fiber and carbon fiber [28–34]. Dandliker et al. have firstly fabricated the tungsten and carbon-steel continuous wire reinforced Zr-based BMGMCs by quenching the metallic melt to a glass after infiltrating the reinforcement [28]. The continuous long fibers in the glass matrix can efficiently hinder the propagation of main shear bands, improving the plastic strain from 0% of monolithic BMG to over 2% of those reinforced with steel wires. Kim et al. have successfully fabricated carbon
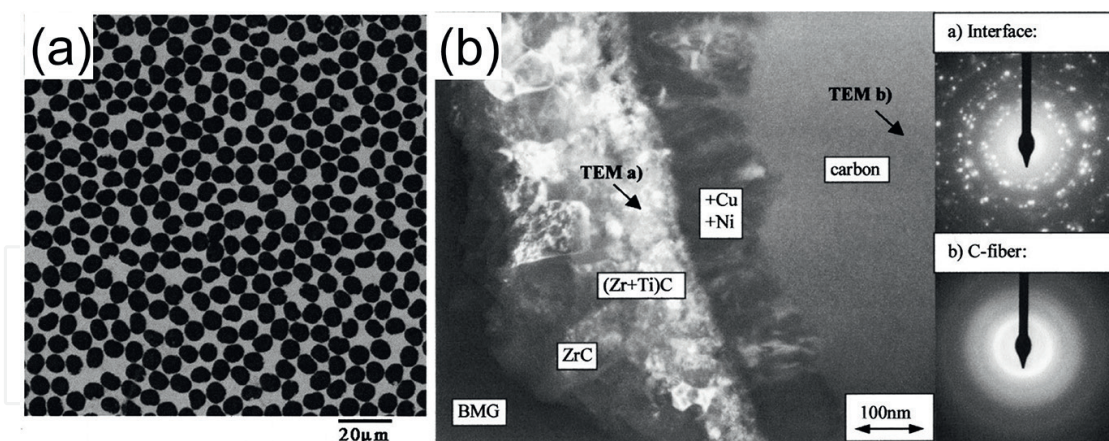
Figure 3. (a) Backscattered SEM image of carbon fiber reinforced bulk metallic glass composite; (b) dark field TEM of the interfacial region between a carbon fiber and the matrix.

fiber reinforced Zr-based BMGMCs by infiltrating the alloy melt to the bundle of carbon fibers in a quartz tube which are cleaned and preheated [30]. **Figure 3a** shows the backscattered SEM image of the carbon fiber reinforced composite. The carbon fibers are uniformly distributed in the matrix and the matrix appears to be uniform and free of heterogeneity. The volume fraction of carbon fibers is about 50% and the diameter is about 5 μm. They also found that a carbide reaction zone is formed surrounding the carbon fibers, as shown in **Figure 3b**, starting from the carbon fibers, a diffusion zone of Ni, Cu within the fiber, a crystallize reaction zone of (Zr + Ti)C and ZrC, to the BMG matrix. Qiu et al. cast the sample in a resistive furnace by melting the ingots in an evacuated quartz tube packed with the tungsten fibers, followed by pressure infiltration [34]. After pressurization the tube was quenched in a supersaturated brine solution. The nominal diameter of the fibers is 250 μm. The volume fraction of the fibers varies from 10 to 70%.

During compression test, unlike the catastrophic fracture of monolithic BMG, the composites reinforced with tungsten fibers shows yielding and plastic deformation. The yielding strength also increases with a higher volume fraction of fibers. They also found that the failure mode changes with various volume fractions of fibers. The monolithic glass fractures on 45° planes. As the volume fraction of fiber increases, failure mode shifts from shear to localized buckling and tilting.

2.2. Particle-reinforced BMGMCs

The particle-reinforce BMGMCs includes ceramic particles, metal particles and the matrix includes Zr-based, Ti-based and Mg-based alloy system [35–43].

Choi-Yim and Johnson have firstly introduced ceramic particle such as SiC, WC and TiC, and the metal particles W and Ta into Zr-based and Cu-based BMG matrix [35]. A mixture of the pre-alloyed metallic glass forming elements and secondary phase material are combined by induction melting the glass forming alloy together with the solid secondary phase material on a water-cooled copper boat under a Ti-gettered argon atmosphere. The volume fractions of particles range from 5 to 30% and the sizes of the particles vary between 20 and 80 μm. **Figure 4**
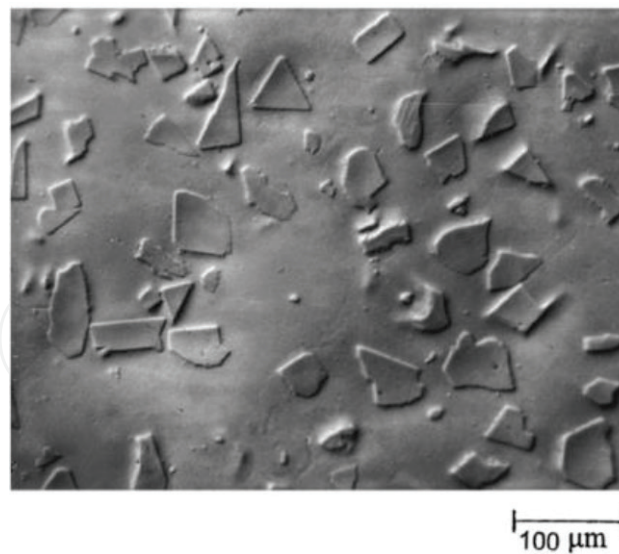
Figure 4. An optical micrograph showing uniformly distributed WC particles in the matrix.

shows the uniformly distributed WC particles in the metallic glass matrix with the volume fraction of 10%. The matrix composition is chosen for several reasons. A relatively low melting temperature suppresses the chemical interactions between the reinforcement particles and the glass. A low glass transition temperature decreases differential thermal stresses which arise between the reinforcement and the matrix during freezing and cooling.

Zhang et al. have introduced Ta particles into Zr-Cu-Al-Ag BMG matrix, the average size of Ta particles is about 40 μm and the volume fraction varies from 5 to 20% [36]. The composite is prepared by induction melting the Zr-Cu-Al-Ag alloy together with Ta powder in a quartz tube and subsequently injecting through a nozzle into a copper mold. **Figure 5a** shows the SEM images of the as-cast BMGMCs containing 10% Ta, consisting of homogeneously dispersed particles embedded in the metallic glass matrix. **Figure 5b** shows the compressive stress-strain curves of the composites containing 5–20% Ta. The monolithic glassy alloy fails immediately after yielding at 1885 MPa. However, the composites exhibit apparent work hardening and plastic strain. For 10% Ta-containing composite, the yield strength, fracture strength and plastic strain are 1717, 2600 MPa and 31%, respectively. The composite containing 20% Ta shows no plasticity which may originate from the crystallization of the matrix. Ta particles play an important role in the initiation and propagation of the multiple shear bands. The differences in Young's modulus between Ta particles and glassy matrix generates high-stress concentration occurs at the interfaces, which promotes the initiation of shear bands at the interface prior to the formation of shear bands on the maximum shear surface.

Pan et al. have added Nb particles into Mg-based BMG matrix to fabricate the ex-situ particle-reinforced BMGMCs [43]. The size of Nb particles is 20–50 μm, the volume fraction varies from 4 to 8%. The particles are added during inductively melting the master alloy. The composite alloy is remelted by induction in a quartz tube and injected with argon pressure into copper molds. **Figure 5c** shows the SEM micrograph of the cross-sectional surface of the composite with 8% Nb particles, which exhibits the uniform distribution of the particles
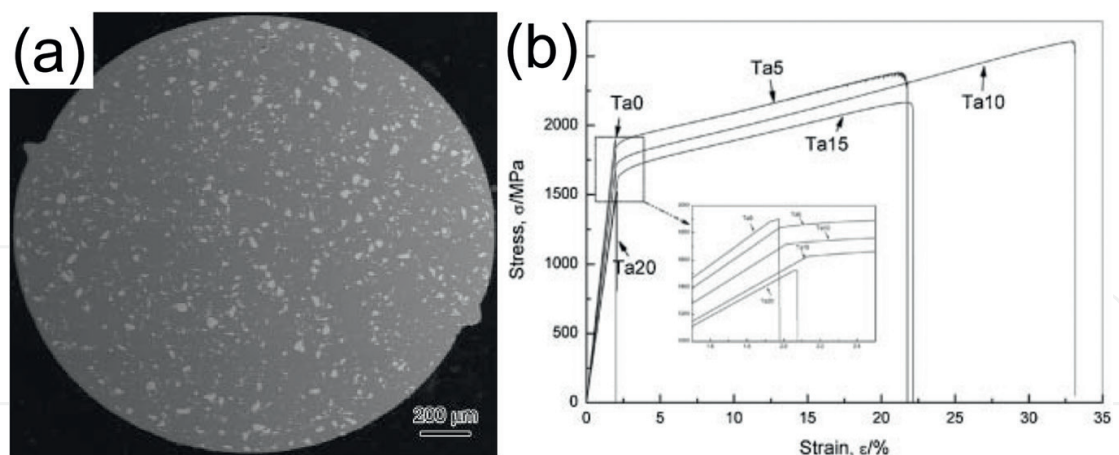
Figure 5. (a) SEM image of the as-cast BMGMC containing 10% Ta; (b) compressive stress-strain curves of the BMGMCs containing 0–20% Ta; (c) SEM image of the composite containing 8% Nb (inset shows the XRD pattern); (d) compressive stress-strain curves for single phase BMG and Nb-containing composite (4 and 8%).

without interfacial reaction. **Figure 5b** shows stress-strain curves for monolithic BMG and Nb-containing composite with 4 and 8% Nb particles. The BMG fails just after the elastic limit of 2%, but the composites yield at about 900 MPa and exhibit significantly plastic strain as well as work hardening and softening. The overall engineering plastic strain is determined to be about 12.1% for 8% Nb-containing composite. Ductile Nb particles serve as obstacles to impede shear bands propagation. When encountering an Nb particle, the shear band has to be either blocked or bypass around the particle due to the strong bonding between the particles and the matrix. Furthermore, if the sear deformation travels into the ductile Nb particles, the particle can dramatically plastic deform by dislocation mode to absorb the shear strain and prevent the catastrophic failure from taking place by the free propagation of unstable shear bands.

2.3. Other kind of ex-situ BMGMCs

Besides fiber and particle reinforcement, recently, some new kind of secondary phases have been introduced to BMG matrix, such as pores and porous particles [43–46].

Wada et al. introduced pores into Pd-based BMG matrix [44]. The master alloy melts are subjected to four distinct hydrogenation treatments at 853 K in tubes of fused silica: (i) 12 h at 1 MPa, then oil quench, (ii) the same, then water quench; (iii) 3 h at 4 MPa, then oil quench, and (iv) the same, then water quench to form porous rods. The porosities of BMG rods are calculated to be 1.7–3.7% from their density. The pore size is observed to be 20–30 μm, as shown in **Figure 6a**. The stability of the fine uniform pore distribution during casting follows from the high viscosity of the melt. Compressive stress-strain curves are strongly affected by porosity, as shown in **Figure 6b**. The porous alloy with the highest porosity of 3.7% shows the plastic strain over 18%, greatly enhanced compared to the pore-free BMG. But during tension, no plasticity can be observed. The shear band pattern is affected by the pores acting as stress concentrators. The pores are comparable in radius with the notch roots giving enhanced toughness, and are expected to induce extensive shear banding.
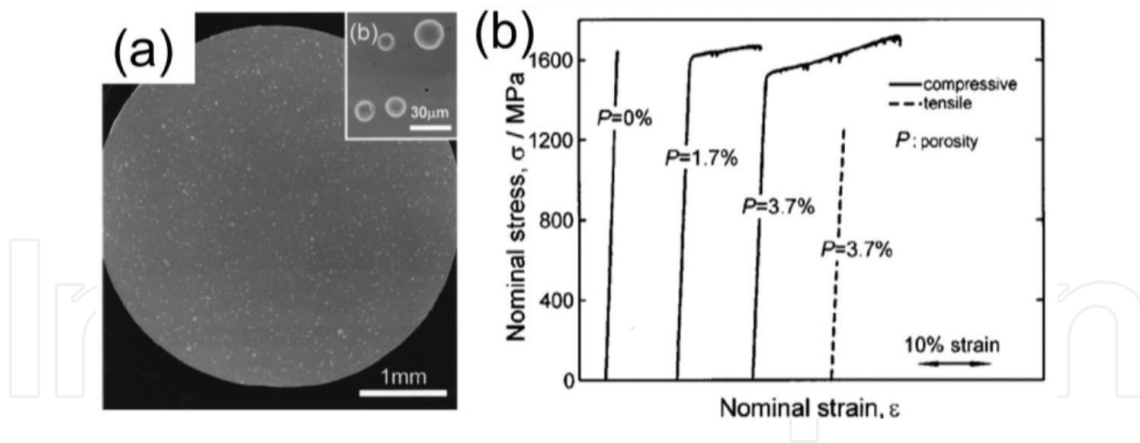
Figure 6. (a) Pore distributed BMG rods, water quenched from a melt held at 853 K for 3 h under 4 MPa hydrogen; (b) tensile and compressive stress-strain curves of pore reinforced BMGMCs with different porosities.

Jang et al. have introduced porous Mo particles into Mg-Cu-Gd-Ag BMG matrix [45]. During master alloy melting, high purity porous Mo particles with a spherical shape and a size of 20–70 μm are added in the matrix alloy. The volume fraction of porous Mo particles ranges from 10 to 25%. For the introduced porous particles, the overall microstructure of the composite is separated into larger-scale compartment, ~50 μm between Mo particles, and the fine-scale compartment, 1–5 μm within one porous Mo particle, as shown in **Figure 7a** and **b**. The composites containing 20–25 vol% porous Mo particles exhibit superior mechanical performance with ultimate compression stress up to 0.95 and 1.1 GPa and plastic strain up to 10%, as shown in **Figure 7c**. Unlike solid particles, the crack propagation in the present composite is arrested by the porous Mo particles. For the porous nature of the reinforcing phase, the numbers of particles are calculated to be 1.4 times higher than those with solid ones, i.e., the mean interspacing of the porous Mo particles is less than that of the solid Mo ones. This should favor to the confining the shear-banding behavior, thus enable more halting propagation of the shear bands. The porous Mo particles separates and restricts the highly localized shear banding into many isolated small regions, and can confine lots of microsized compartments of the matrix within porous particles, which results in the formation of multiple shear bands within or around the porous particles, promoting the deformation to distribute more uniformly across the sample.

Guo et al. have used an original method, so-called top-down process, to fabricate porous NiTi shape memory alloy (SMA) powders [46]. In this process, the multiphase precursor powder of Ni-Ti-Gd is firstly produced with B2-NiTi and Ni-Gd phase, then by leaching in nitric acid solution to remove Ni-Gd phase and leaving pore in the powder, as shown in **Figure 8a**. The size and interspacing between NiTi within one porous particle are as small as 200 nm. The porous NiTi powders are subsequently added to Mg-Cu-Gd-Ag glass former liquid to fabricate the BMGMC, as shown in **Figure 8b**, with volume fraction ranged from 5 to 20%. The porous particles are homogeneously distributed in the glassy matrix. The composites containing 20 vol% porous NiTi particles exhibits the best mechanical properties, including a true plastic strain of up to 10.6% and a fracture stress of up to 1173 MPa, as shown in **Figure 8c**. Similar to porous Mo, many microcracks are confined in the inter-particle regions and should result from local shear banding within the amorphous matrix. Furthermore, compared with solid particles, the porous particles can generate
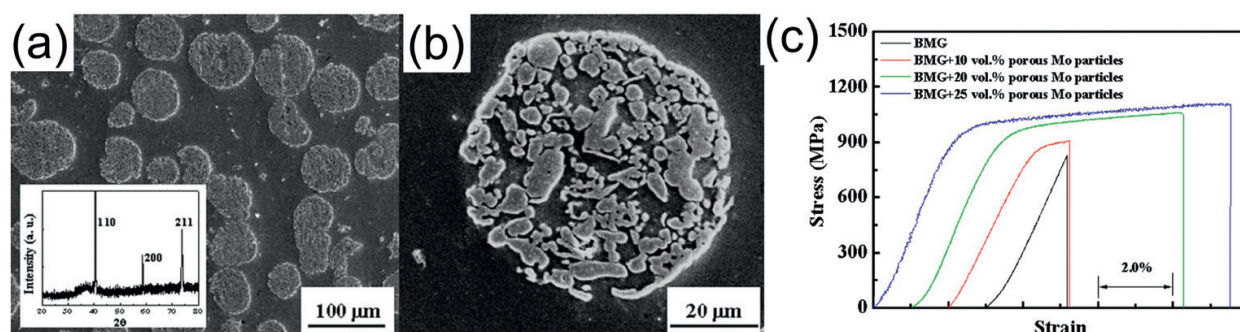
Figure 7. (a) SEM observation of the porous Mo particles in the BMG matrix, with the inserted XRD pattern; (b) an enlarged image of a single porous Mo particle; (c) representative room-temperature compressive engineering stress-strain curves for the BMGMCs.
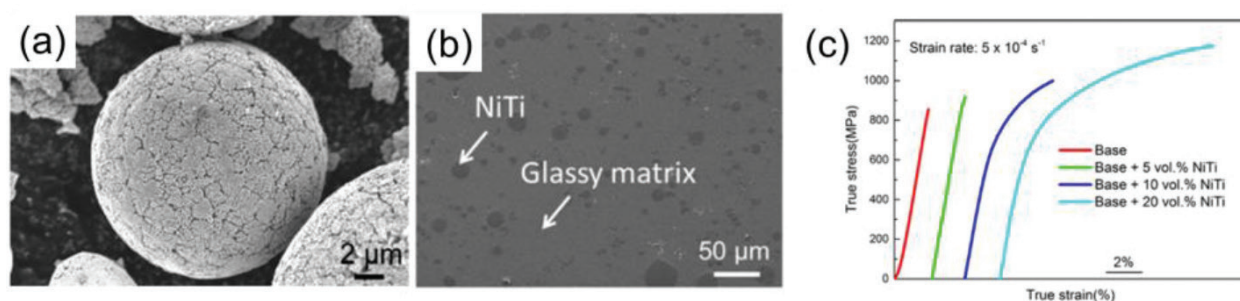

Figure 8. (a) Porous NiTi powder by top-down process; (b) SEM images of BMGMCs containing 20 vol% porous particles; (c) compressive true stress-strain curves for monolithic base BMG and BMGMCs with various volume fraction of porous NiTi addition.

more interfaces, which makes the yield strength follows the load-bearing mode even with low volume fraction of particles. This composite also shows very obvious work hardening behavior, which is considered to originate from the stress-induced martensitic transformation of B2-NiTi phase, which is very attractive and different from those conventional metal or ceramic particles.

3. In-situ BMGMCs

For in-situ BMGMCs, the fabrication process is very important and difficult to design, such as how to induce in-situ precipitated phase, how to control the volume fraction and size of secondary phase. For different alloy systems, the process and reinforcing phases are quite different, thus, this part will be divided by alloy systems, not by reinforcing phases.

3.1. Zr-based BMGMCs

β-Zr phase is one of the in-situ reinforcements in Zr-based BMGMCs that has been studied a lot. Hays et al. have reported the development of β phase reinforced Zr-Ti-Cu-Ni-Be-Nb BMGMCs [47]. Both XRD patterns and SEM images suggest the precipitation of β phase during rapid quenching. The β phase is in the dendritic and distributed in the glassy matrix homogeneously, as shown in **Figure 9a**. The volume fraction of β phase is estimated to be ~25%. The dendritic

structures are characterized by primary dendrite axes with lengths of 50–150 μm and radius of about 1.5–2 μm. Regular patterns of secondary dendrite arms with spacing of 6–7 μm can be observed from SEM images. This composite shows about 5% plastic strain under three point bending. **Figure 9b** shows that the shear bands propagate preferentially through many successive dendrite arms, occasionally initiate or terminate within the arms, and clearly propagate as localized bands through the β-phase arms. This composite also shows good plasticity during compression, as shown in **Figure 9c**. It yields at 1.3 GPa when the β phase yields and deforms, and shear band patterns develop, as the glassy matrix is locally loaded beyond its critical shear stress. The plastic strain is over 6%. The composite even shows about 5% plastic strain during tension. Clear necking and deformation can be observed. The dendritic microstructure of the β phase acts to seed the initiation of organized shear band patterns, confines the propagation of individual shear bands to domains having a spatial scale of the order of the primary dendritic axes length, and lead to shear band spacing which is related to the dendrite arm spacing.

Another important in-situ secondary phase in Zr-based BMGMCs is refractory metal phase. Fan et al. have introduced in-situ Ta-rich precipitates in Zr-Cu-Al-Ni-Ta BMGMCs [48]. For the high melting temperature of Ta, there are two steps arc-melting during master alloy preparation. Firstly, Zr-Ta ingot is fabricated which forms solid solutions of Zr-Ta, and remaining elements are subsequently mixed with Zr-Ta ingots. The microstructure of the as-cast composite samples consists of both glassy matrix and Ta-rich particles with an average size of 10–30 μm, as shown in **Figure 10a**. The particles are oblong in shape and do not appear to possess a dendritic structure, they distribute homogeneously among the matrix and the volume faction is about 4%. This composite yields at 1.7 GPa and exhibits apparent work hardening and significant plastic strain, as shown in **Figure 10b**. The elastic incompatibility between the particles and the matrix introduces stress concentrations which may promote shear band initiation. The particles may also impede shear band propagation. Guo et al. have applied dealloying in metallic melt method to further optimize the microstructure and mechanical properties of Ta-rich phase reinforced BMGMCs [49]. The dealloying in metallic melt phenomenon occurs when immerging Zr-Ta solid solution precursor in Cu-Al-Ni melt. For the negative enthalpy of mixing between Zr and Cu-Al-Ni and positive enthalpy of mixing between Ta and Cu-Al-Ni, Zr is gradually selectively leached from precursor ingot to
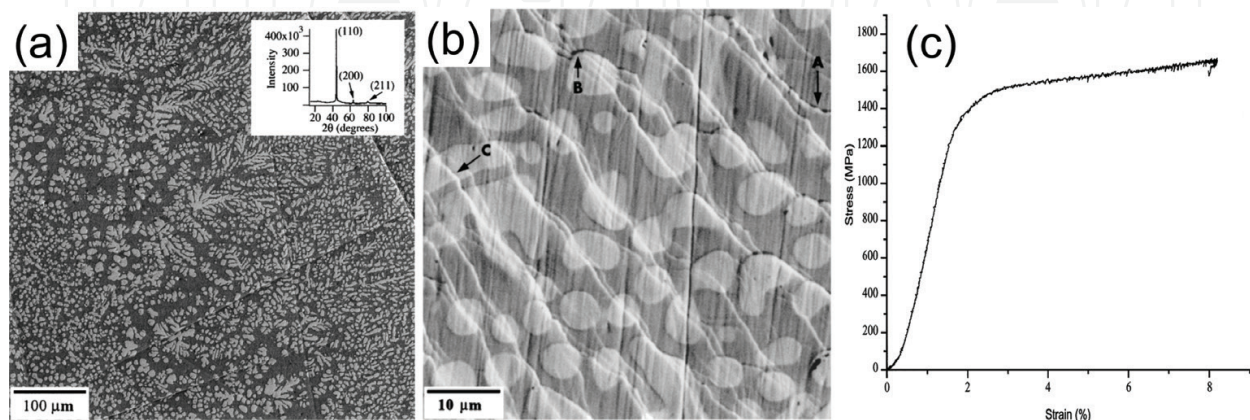

Figure 9. (a) SEM image of in-situ β-Zr reinforced BMGMCs (inset: XRD patterns); (b) shear band patterns array from compressive failure region of bend test sample; (c) compressive stress strain curve for the composite.
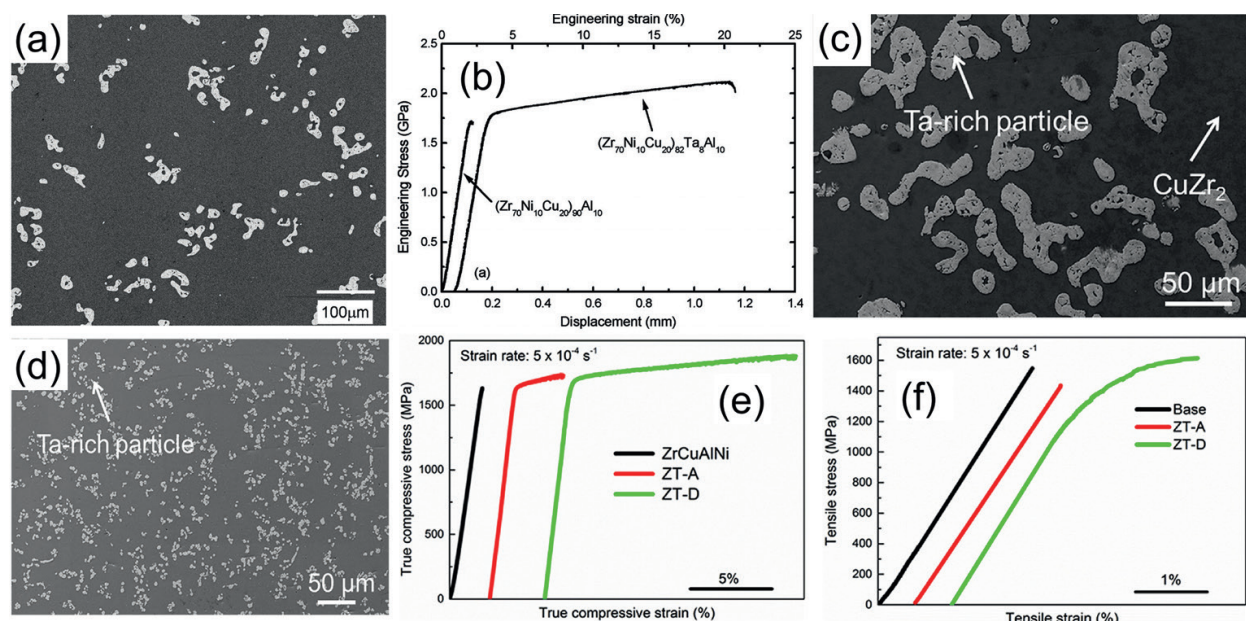
Figure 10. (a) SEM image of in-situ Ta reinforced BMGMCs; (b) compressive stress-strain curves for as-cast in-situ Ta reinforced BMGMCs; (c) SEM images of the sample by conventional arc-melting; (d) SEM images of the sample by novel dealloying method; (e) true compressive stress-strain curves and (f) tensile stress-strain curves of monolithic BMG, BMGMC by arc-melting (ZT-A) and BMGMC by dealloying (ZT-D).

the melt and forming a glass-former liquid, while at the same time, remaining Ta breaks into small particles and distribute in the melt. By finally quenching, the BMGMCs can be fabricated. Interestingly, the size of Ta-rich particles by dealloying method is much smaller than that by conventional arc-melting method, 40 μm of arc-melting sample and 10 μm of dealloying sample, as shown in **Figure 10c** and **d**.

The reason is considered to be that during conventional arc-melting, the Ta-rich particles precipitate during cooling and its size can be hardly controlled, while during dealloying, for the low melting temperature, the Ta-rich particles remain in solid state and finally fine particle can be obtained. With these finer particles, the composite by dealloying method shows better plasticity than that by arc-melting method under both compression and tension, as shown in **Figure 10e** and **f**. The plastic strain for arc-melting sample is 3% under compression and 0% under tension. However, the value for dealloying sample is 14% under compression and 1.8% under tension. As discussed before, the stress concentration at the interfaces between Ta-rich particles and glassy matrix contributes a lot to the overall plasticity. For the finer size of particles in dealloying samples, the number density of particle and equivalent interface area per mm^3 are quite larger than arc-melting sample, 34.4×10^4, 108 mm^2 for dealloying sample and 0.4×10^4 and 22.5 mm^2 for arc-melting sample. Thus, the five times larger area of interfaces in dealloying sample can plasticize the sample more.

Recently, B2-CuZr shape memory secondary phase in Zr-based BMGMCs have attracted a lot of interests. Unlike conventional metal or ceramic reinforcing phases, the shape memory phase can undergo the stress-induced martensitic transformation during deformation, which can both further improve the plasticity and give the sample obvious work hardening behavior [50]. Xu et al. have induced B2-CuZr phase in Zr-Cu-Al-Co system, as shown in **Figure 11a** [51]. The
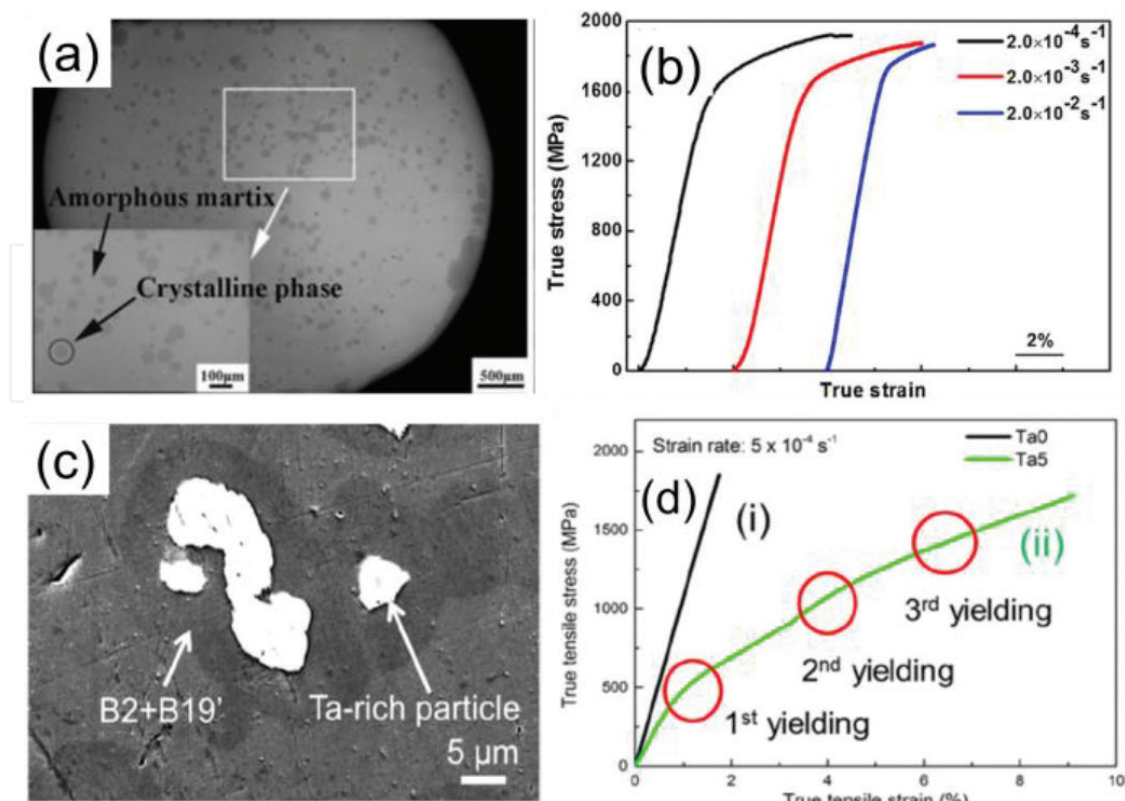
Figure 11. (a) Typical OM images of the B2-CuZr reinforced BMGMCs (inset: enlarged parts of rectangular area); (b) true stress-strain curves of the composites with various strain rates; (c) SEM image of ta-doped sample; (d) true tensile stress-strain curves of both monolithic base alloy (Ta0) and Ta-doped multiphase reinforced BMGMC (Ta5).

spheroidal crystal phases of B2-CuZr (confirmed by XRD, not shown here) are embedded in the amorphous matrix. The volume fraction of B2-CuZr is estimated to be about 10%. The composite exhibits obvious plastic deformation under compression with various strain rates, as shown in **Figure 11b**. Moreover, the flow stress increases with the increasing strain after yielding, exhibiting obvious work-hardening behavior. Even though the B2-CuZr reinforced Zr-based BMGMCs have shown good plasticity and work-hardening, but the inhomogeneous distribution of B2-CuZr limits the further improvement of the mechanical properties. During cooling, the B2-CuZr phase tends to precipitate in the center of the sample where the cooling rate is lower than that near the edge. Guo and Saida have successfully homogenized the distribution of B2-CuZr phase by minor doping Ta [52]. During cooling, the primary precipitated Ta-rich phase acts as effective nucleants that promoted copious nucleation of the B2-CuZr phase. As shown in **Figure 11c**, the dark phase of shape memory phase forms around the gray phase of Ta-rich particle. The total volume fraction of crystalline secondary phase, including both Ta-rich particles and B2-CuZr (some transforms to B19'-CuZr because of the residual heat at the interface), is estimated to be ~80% by comparing the heat of crystallization of both the composites and monolithic BMG. The volume fraction of Ta-rich particles is estimated to be ~10% based on the image analysis. This composite shows a superior plasticity of 8.4% plastic strain during tension, as well as obvious work-hardening and a unique triple yielding phenomenon, as shown in **Figure 11d**.

3.2. Ti-based BMGMCs

The shape memory phase has also been introduced into Ti-based BMGMCs. Hong et al. have successfully induced B2 phase in Ti-Cu-Ni-Zr-Sn-Si system [53]. The size and distribution of B2 phase can be also tailored by varying the composition, as shown in **Figure 12a** and **b**. The size of B2 phase varies from 2–5 to 70–150 μm. The volume fraction varies from 10 to 33%. The composites also shows good plasticity under compression, the largest plastic strain is about 12.7%, as shown in **Figure 12c**. Furthermore, the yield strength exhibits a tendency to decrease with the increase of volume fraction of B2 phase, which originates from the early deformation on softer B2 phase. However, the plastic strain increases with more and larger B2 phase. The large B2 phase is found to be effective in dissipating the localization of shear stress, thus causing branching and multiplication of the shear bands. It is also observable that the severe deformation in the B2 phase, formation of wrinkles suggesting the possible deformation-induced phase transformation, as shown in **Figure 12d**.

Another important reinforcement in Ti-based BMGMCs is the β phase. Very good plasticity can be even observed for such composites under tension [54]. However, most of these composites contains Be, which is toxic and should be avoided when used as biomaterials. To induce β phase in Be-free alloy system, the β phase stabilizers, such as Ta, V and etc. Yamamoto et al. have successfully induced β-Ti phase in Ti-Cu-Ni-Sn-Ta system [55]. As shown in **Figure 13a**, for the low glass-forming ability of the matrix, Ti_2Ni also forms besides β-Ti phase. Thus, the plasticity of this composite is not very good, the plastic strain is about 1.6%, as shown in **Figure 13b**. To further improve the mechanical property, Guo and Kato have chosen a better glass former, Ti-Zr-Cu-Pd-Sn alloy, and used Mo as the β-Ti phase stabilizer element [56]. By doping 2 at%
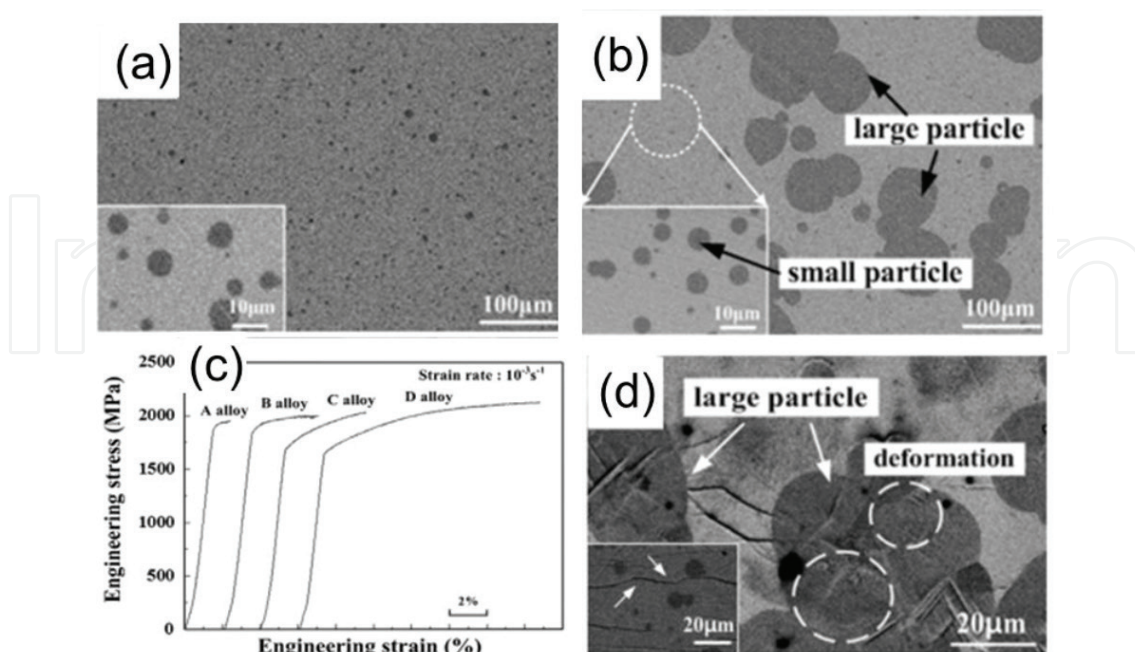

Figure 12. (a) and (b) SEM images of B2 phase reinforced Ti-based BMGMCs with different composition; (c) stress-strain curves of B2 phase reinforced Ti-based BMGMCs; (d) SEM image from the lateral surface of fractured sample.
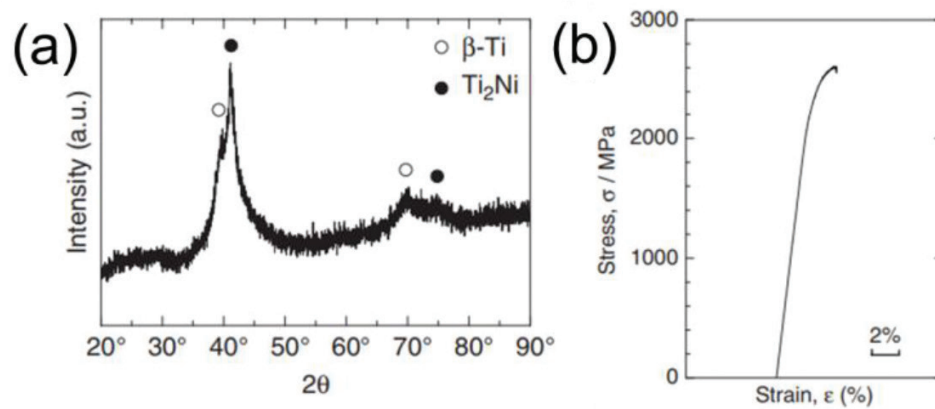
Figure 13. (a) XRD patterns and (b) stress-strain curves under compression for β phase reinforced Ti-Cu-Ni-Sn-Ta BMGMCs.

Mo, homogeneously distributed oblong-like β-Ti phase can be observed from **Figure 14a**. The volume fraction and average size of β-Ti are estimated to be about 25 μm and 25%. This composite also shows a good plasticity under compression, fracture strength of 2160 MPa and plastic strain of 13.4%, as shown in **Figure 14b**. The nanoindentation test has shown that the β-Ti phase is softer than the matrix, indicating the propagation of the main shear band is hindered by the interfaces between the softer β-Ti and glassy matrix. The shear band is deflected, branched, or multiplied. Furthermore, after elastic deformation of both β-Ti and matrix to the yielding point, the β-Ti appears to yield and deform, contributing to the work-hardening behavior. The composite also shows about 3% plastic strain under three point bending test, see **Figure 14c**.

3.3. Mg-based BMGMCs

The researches on in-situ Mg-based BMGMCs are not as much as those in Zr-based or Ti-based systems for the difficulty to design proper fabrication process. However, recently, the application of novel dealloying in metallic melt method or selective phase leaching method in fabrication of in-situ Mg-based BMGMCs have attracted a lot of attentions.
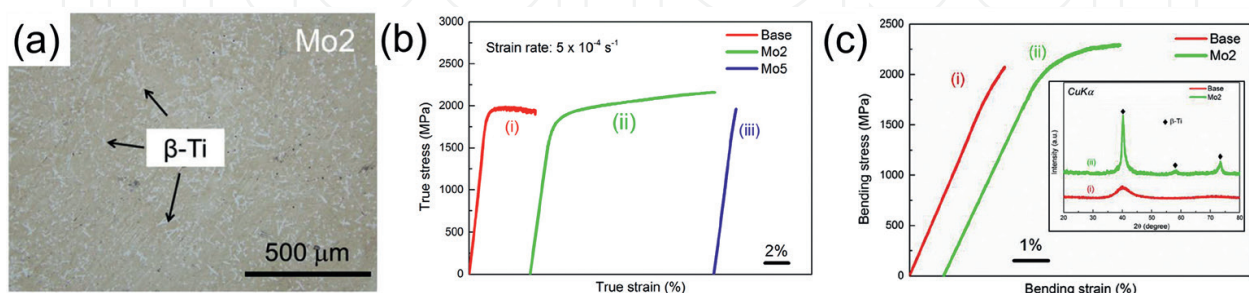

Figure 14. (a) OM image of Mo-doped β-Ti based BMGMCs; (b) compressive true stress-strain curves for both monolithic base alloy and Mo-doped BMGMCs; (c) bending stress-strain curves for both base alloy and BMGMCs (inset: XRD patterns for bending samples).

Oka et al. have successfully introduced α-Ti phase in Mg-Cu-Gd BMG system by using novel dealloying in metallic melt method [57]. The schematic of this method is shown in **Figure 15a**. For the negative value of heat of mixing (miscible) between Ti-Cu and Gd-Cu while positive value (immiscible) of Ti-Gd, Ti-Cu and Gd-Cu phases are expected to form in the prealloy. Similarly, for the negative value of heat of mixing between Mg-Gd and Mg-Cu while positive value of Mg-Ti. When the Ti-Cu-Gd prealloy consisting of Cu-Gd and Ti-Cu phases is immersed in the Mg-melt, the Cu-Gd phase and Cu dealloyed from the Ti-Cu phase are expected to dissolve. They will form the Mg-Cu-Gd BMG formable liquid if the Mg, Cu and Gd proportions are correctly balanced. The remaining elemental Ti from Ti-Cu phase is thought to form the porous structure by a surface diffusion mechanism in the Mg-Cu-Gd alloy liquid. Rapid cooling of the semi-solid mother alloy yields Mg-Cu-Gd BMG with in-situ Ti dispersoids, as shown in **Figure 15b**. By using this strategy, the in-situ Ti dispersoids have been successfully introduced. Furthermore, for the Ti dispersoids are directly dealloyed from Ti-Cu phase, thus, the size of them can be reduced by decreasing the size of Ti-Cu phase. By increasing the cooling rate of Ti-Cu-Gd prealloy, the Ti-Cu phase is refined and subsequently the size of Ti dispersoids also decreased. As shown in **Figure 15c**, during four point bending test, the composite with large and fine Ti dispersoids shows a fracture strength of 230 and 387 MPa, 6 and 78% higher than the monolithic BMG, respectively. With fine pore Ti dispersoids, the size and inter-particle spacing of Ti phase is estimated to be ~500 nm, which is very close to the characteristic plastic processing zone size of reported Mg-based BMG, 100–1000 nm. Thus, optimum condition for the composite effect has locally achieved within and surrounding the porous Ti dispersoids. Therefore, these regions and surrounded area of glassy near porous Ti could deform plastically. However, for the low volume fraction of Ti dispersoids (~2%), macroscopic plasticity is not obtained in this system. Subsequently, Guo et al. have applied similar dealloying reaction in Mg-Cu-Gd-Ag system with better glass-forming ability [49]. As shown in **Figure 16a**, homogenous distributed α-Ti phase among the glassy matrix can be observed. The average size and volume fraction are estimated to be about 6 μm and 13%, respectively. This composite shows improved mechanical properties compared with its monolithic counterpart,
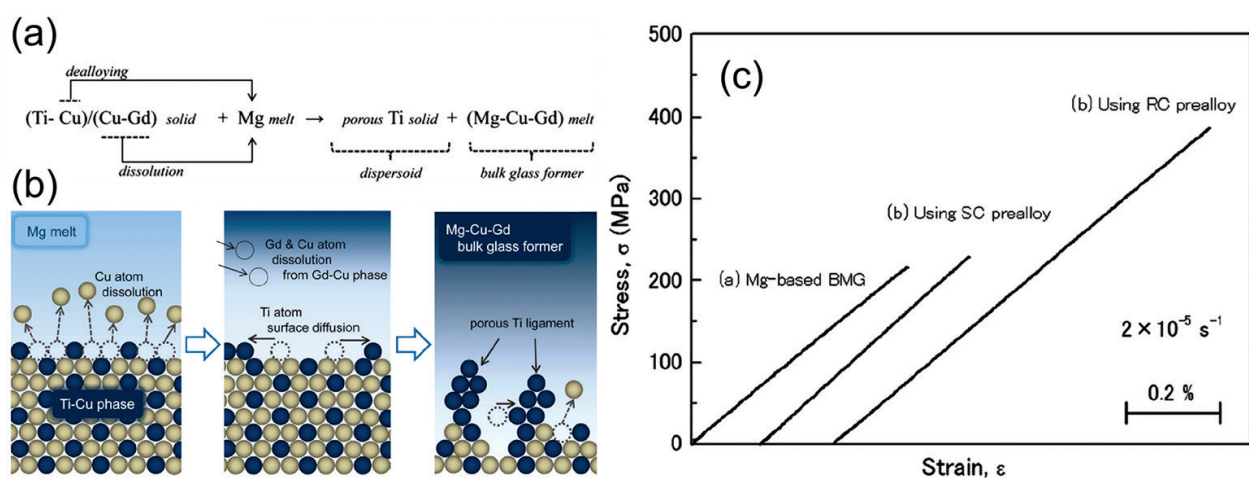

Figure 15. (a) Schematic showing porous Ti formation by dealloying in metallic melt; (b) schematic showing the preparation of the mother alloy; (c) stress-strain curves of BMGMCs using rapid cooling prealloy and slow cooling prealloy, under four point bending test.
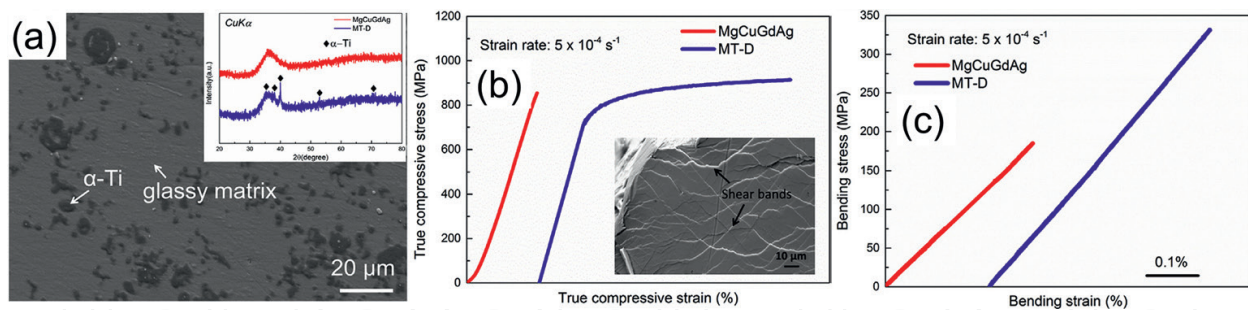
Figure 16. (a) SEM images of in-situ Ti reinforced Mg-based BMGMC by dealloying method (inset: XRD patterns of both BMGMC and its monolithic counterpart); (b) true compressive stress-strain curves of both BMGMC and its base alloy (inset: SEM images of fractured BMGMC); (c) stress-strain curves by four point banding test.

that is, ~6.1% of plastic strain and 920 MPa of fracture strength during compression test, see **Figure 16b**. The stress concentration at the interfaces between Ti dispersoids and surrounding matrix is in favor of initiating multiple shear bands. Furthermore, when the stress exceeds the yield strength of Ti, it can release the stress concentration condition. The suppression of propagation of the single main shear band is enhanced by such yielding, which causes branching, blocking or multiplying the shear bands. It is therefore, the sample is deformed with a significant plasticity. The composite also shows improved fracture stress and strain during four point bending test, 331 MPa of fracture stress and 0.42% of fracture strain, as shown in **Figure 16c**. The calculated fracture toughness of this composite is ~1.73 MPa m$^{1/2}$, 45% higher than its monolithic counterpart. However, it is still low and cannot lead to plasticity during bending.

As stated above, the shape memory phase has attracted a lot of interest recently for its unique stress-induced martensitic transformation behavior. However, the research on shape memory phase reinforced BMGMCs mainly focus on Zr-based or Ti-based BMGMCs. Guo and Kato have successfully induced in-situ B2-NiTi shape memory phase in Mg-Ni-Gd-Ag BMGMCs by using novel selective phase leaching in metallic melt method [58]. A schematic of the novel designed process is shown in **Figure 17a**, which contains roughly three steps: Ni-Ti-Gd precursor preparation by arc-melting, master alloy preparation by induction melting and composite preparation by copper mold casting. From the Ni-Ti, Ti-Gd and Ni-Gd phase diagrams, it is possible to prepare a Ni-Ti-Gd ternary precursor consisting of only NiTi and Ni-Gd phases if the proportions of Ti, Ni, and Gd are properly balanced. Then, the temperature of master alloy preparation is kept low enough for NiTi dispersoids not to melt or dissolve, but high enough for the Ni-Gd phase to dissolve into the Mg-Ag melt, owing to their different reactivities. Moreover, the amounts of Mg-Ag melt and dissolved Ni-Gd was properly balanced to form the glass-forming matrix. Finally, Mg-based BMGMCs, an Mg-Ni-Gd-Ag BMG matrix with in-situ NiTi dispersoids, is fabricated by casting this semi-solid melt into a copper mold. By using such strategy, the in-situ B2-NiTi phase have been successfully induced, as shown in **Figure 17b**, the average size is ~8 μm and the volume fraction is ~15%. As shown in **Figure 17c**, the composite shows a higher fracture stress (~906 MPa), plastic strain (~7%), and work hardening than its monolithic counterpart. The shear bands were considered to be obstructed by the in-situ ductile NiTi dispersoids, which deflected their propagation and caused branching or multiplying of the shear bands, typically observed in ductile metal reinforced BMGMCs and is known as the "blocking effect". Moreover, a stress-induced phase transformation from
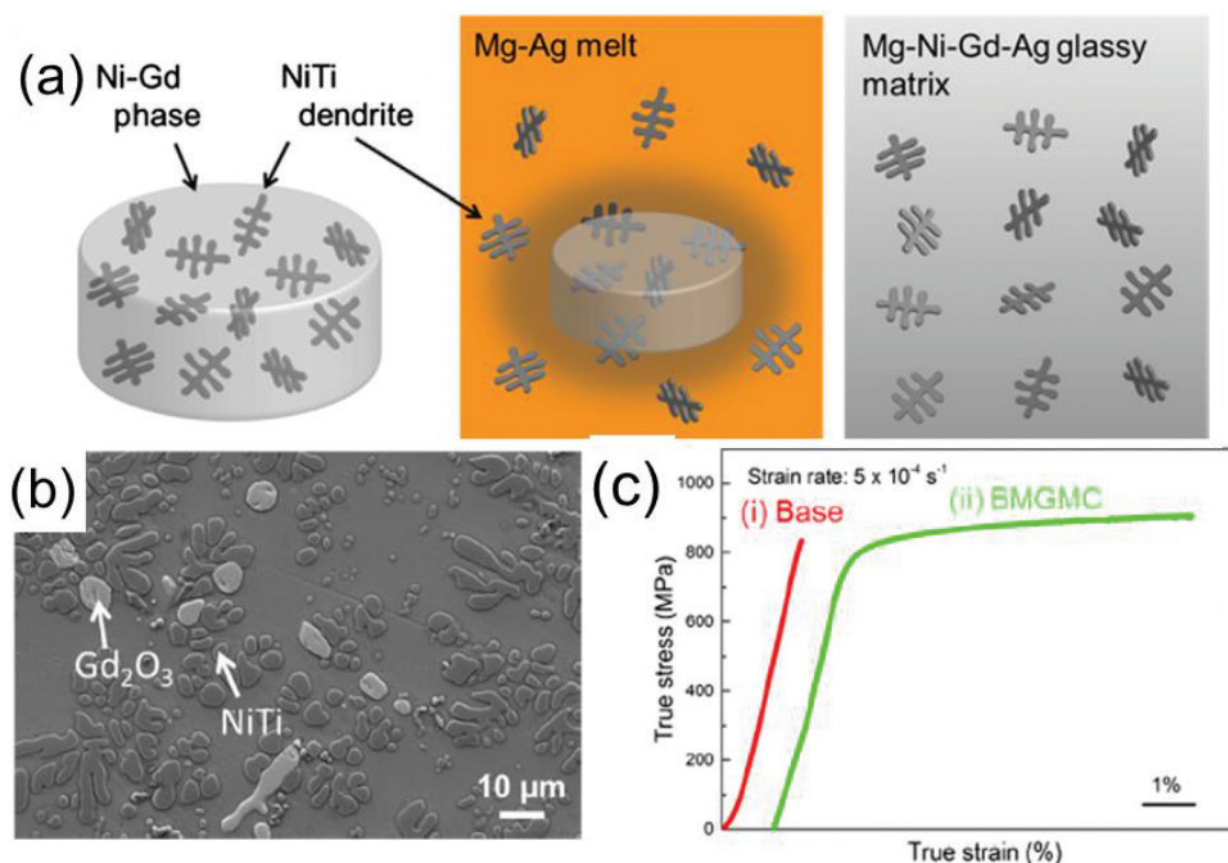
Figure 17. (a) Schematic of the fabrication process; (b) SEM image of B2-NiTi reinforced mg-based BMGMC; (c) compressive true stress-strain curves for both base alloy and BMGMC.

B2-NiTi to B19'-NiTi during deformation releases the stress concentration around the dispersoids to restrict free volume accumulation. This process hindered the rapid propagation of shear bands, meaning that additional stress was required to move the shear bands, called the "TRIP effect". Since the B2-NiTi phase precipitates during Ni-Ti-Gd precursor preparation and has no change from then on, the size of it can be refined by increasing the cooling rate of the precursor. Thus, the precursor rods by tilt casting technique are produced with various diameters, i.e., various cooling rate. With a higher cooling rate, the size of B2-NiTi is smaller, from 8 to 2 μm, as shown in **Figure 18a** and **b**. With finer B2-NiTi phase, the composite shows higher fracture strength and larger plastic strain, as shown in **Figure 18c**. The sample with finest particle size exhibits the best mechanical properties, i.e., 1096 MPa fracture strength and 15.5% plastic strain. The volume fraction of the B2-NiTi phase has also been improved by adjusting the composition with higher Ti amount. The volume fraction increases from 15 to 32% and the optimized composite shows superior plasticity during compression, as shown in **Figure 19a**, a fracture stress of 1212 MPa and a fracture strain of 25.3%. **Figure 19b** summarizes the compressive property data of various in-situ Mg-based BMGMCs, including Fe, long-period stacking ordered structure (LPSO), NiZr, AgMg, and quasicrystal reinforced composites [59–63]. Both the fracture strength and fracture strain of the optimized B2-NiTi reinforced BMGMC are the highest among all in-situ Mg-based BMGMCs reported to date.
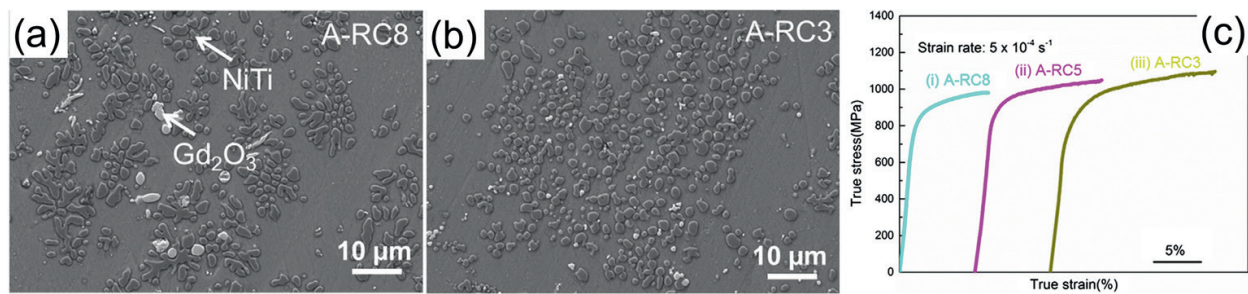
Figure 18. SEM images of the composites using rapid cooling precursor: (a) 8 mm rod precursor; (b) 3 mm rod precursor; (c) compressive true stress-strain curves of the composites using rapid cooling precursor with various diameter, 8, 5 and 3 mm.
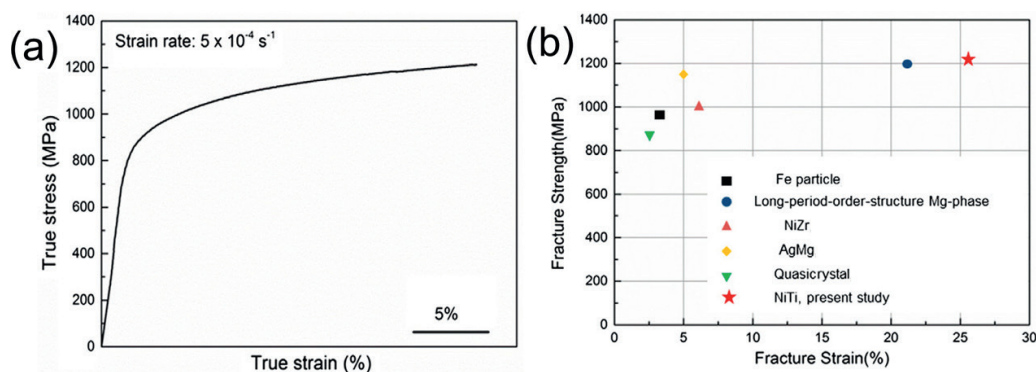

Figure 19. Compressive true stress-strain curves of the optimized B2-NiTi reinforced BMGMCs; (b) fracture strength versus fracture strain for various in-situ Mg-based BMGMCs to date.

4. Conclusion and outlook

In this chapter, both ex-situ and in-situ BMGMCs developed in Zr-based, Ti-based, Mg-based systems have been introduced, such as ceramic particle, metal particle, porous particle reinforced ex-situ BMGMCs and B2-phase, β-phase reinforced in-situ BMGMCs. The microstructures, mechanical properties as well as deformation mechanisms are discussed for each kind of BMGMCs. Compared with nearly zero plasticity of monolithic BMGs, the BMGMCs reinforced by secondary phases show significant improvement in plasticity, e.g., β-phase reinforced Ti-based BMGMCs show over 10% plastic strain under tension, B2-NiTi reinforced Mg-based BMGMCs show over 20% plastic strain under compression, etc. For the limitation of the chapter, more works on various reinforcements and alloy systems cannot be covered. The detailed deformation mechanisms of BMGMCs are not discussed fully either. For further development of BMGMCs, more works should be done on more complex composite structure, the deformation mechanisms, designing novel processing methods, tailoring the microstructures and mechanical properties of the existed BMGMCs. The research on BMGMCs will greatly extend the application potentials of amorphous materials as engineering materials.

Author details

Wei Guo

Address all correspondence to: weiguo@hust.edu.cn

State Key Lab of Materials Processing and Die and Mould Technology, Huazhong University of Science and Technology, Wuhan, China

References

[1] Klement T, Willens R, Duwez P. Non-crystalline structure in solidified gold–silicon alloys. Nature. 1960;**187**:869

[2] Conner RD, Dandliker RB, Johonson WL. Mechanical properties of tungsten and steel fiber reinforced $Zr_{41.25}Ti1_{3.75}Cu12.5Ni_{10}Be_{22.5}$ metallic glass matrix composites. Acta Materialia. 1998;**46**:455

[3] Peker A, Johonson WL. A highly processable metallic glass: $Zr_{41.2}Ti_{13.8}Cu_{12.5}Ni_{10.0}Be_{22.5}$. Applied Physics Letters. 1993;**63**:2342

[4] Inoue A, Fan C, Saida J, Zhang T. High-strength Zr-based bulk amorphous alloys containing nanocrystalline and nanoquasicrystalline particles. Science and Technology of Advanced Materials. 2000;**1**:73

[5] Drehman A, Greer A, Turnbull D. Bulk formation of a metallic glass: $Pd_{40}Ni_{40}P_{20}$. Applied Physics Letters. 1982;**41**:716

[6] Kui H, Greer A, Turnbull D. Formation of bulk metallic glass by fluxing. Applied Physics Letters. 1984;**45**:615

[7] Turnbull D. The liquid state and the liquid-solid transition. Transactions of AIME. 1961;**221**:422

[8] Telford M. The case for bulk metallic glass. Materials Today. Materials Today. 2004:36

[9] Liu C, Heatherly L, Easton D, Carmichael C, Schnerberl J, Chen C. Test environments and mechanical properties of Zr-base bulk amorphous alloys. Metallurgical and Materials Transactions A: Physical Metallurgy and Materials Science. 1998;**29**:1811

[10] Inoue A. Stabilization of metallic supercooled liquid and bulk amorphous alloys. Acta Materialia. 2000;**48**:279

[11] Inoue A, Zhang W, Zhang T, Kurosaka K. Cu-based bulk glassy alloys with high tensile strength of over 2000 MPa. Journal of Non-Crystalline Solids. 2002;**304**:200

[12] Inoue A, Shen BL, Koshiba H, Kato H, Yavari AR. Ultra-high strength above 5000 MPa and soft magnetic properties of Co-Fe-Ta-B bulk glassy alloys. Acta Materialia. 2004;**52**:1631

[13] Inoue A. High Strength Bulk Amorphous Alloys with Low Critical Cooling Rates (Overview). Materials Transactions, JIM. 1995;**36**:866

[14] Schroeder V, Gilbert CJ, Ritchie RO. Comparison of the Corrosion Behavior of a Bulk Amorphous Metal, $Zr_{41.2}Ti_{13.8}Cu_{12.5}Ni10Be22.5$, with Its Crystallized Form Scripta Materialia. 1998;**38**:1481

[15] Chen H, He Y, Shiflet GJ, Poon SJ. Mechanical properties of partially crystallized aluminum based metallic glasses. Scripta Materialia. 1991;**25**:1421

[16] Argon AS, Kuo HY. Plastic flow in a disordered bubble raft (an analog of a metallic glass). Materials Science and Engineering. 1979;**39**:101

[17] Falk ML, Langer JS. Dynamics of viscoplastic deformation in amorphous solids. Physical Review E. 1998;**57**:7192

[18] Lemaitre A. Rearrangements and dilatancy for sheared dense materials. Physical Review Letters. 2002;**89**:195503

[19] Lund AC, Schuh CA. Yield surface of a simulated metallic glass. Acta Materialia. 2003;**51**:5399

[20] Lund AC, Schuh CA. The Mohr–Coulomb criterion from unit shear processes in metallic glass. Intermetallics. 2004;**12**:1159

[21] Johnson L, Samwer K. A universal criterion for plastic yielding of metallic glasses with a (T/T-g)(2/3) temperature dependence. Physical Review Letters. 2005;**95**:195501

[22] Mayr SG. Activation energy of shear transformation zones: A key for understanding rheology of glasses and liquids. Physical Review Letters. 2006;**97**:195501

[23] Zink M, Samwer K, Johnson WL, Mayr SG. Plastic deformation of metallic glasses: Size of shear transformation zones from molecular dynamics simulations. Physical Review B. 2006;**73**:172203

[24] Chen LY, Setyawan AD, Kato H, Inoue A, Zhang GQ, Saida J, Wang XD, Cao QP, Jiang JZ. Free-volume-induced enhancement of plasticity in a monolithic bulk metallic glass at room temperature. Scripta Materialia. 2008;**59**:75

[25] Schuh CA, Hufnagel TC, Ramamurty U. Mechanical behavior of amorphous alloys. Acta Materialia. 2007;**55**:4067

[26] Joo SH, Kato H, Kim HS. Work-Hardening Induced Tensile Ductility of Bulk Metallic Glasses via High-Pressure Torsion. Scientific Reports. 2015;**5**:9660

[27] Chu JP, Greene JE, Jang JSC, Huang JC, Shen YL, Liaw PK, Yokoyama Y, Inoue A, Nie TG. Bendable bulk metallic glass: Effects of a thin, adhesive, strong, and ductile coating. Acta Materialia. 2012;**60**:3226

[28] Dandliker RB, Conner RD, Johnson WL. Melt infiltration casting of bulk metallic-glass matrix composites. Journal of Materials Research. 1998;**13**:2896

[29] Conner RD, Dandliker RB, Johnson WL. Mechanical properties of tungsten and steel fiber reinforced $Zr_{41.25}Ti_{13.75}Cu_{12.5}Ni_{10}Be_{22.5}$ metallic glass matrix composites. Acta Materialia. 1998;**46**:6089

[30] Kim CP, Busch R, Masuhr A, Choi-Yim H, Johnson WL. Processing of carbon-fiber-reinforced $Zr_{41.2}Ti_{13.8}Cu_{12.5}Ni_{10.0}Be_{22.5}$ bulk metallic glass composites. Applied Physics Letters. 2001;**79**:1456

[31] Qiu KQ, Suo ZY, Ren YL, Yu B. Observation of shear bands formation on tungsten fiber-reinforced Zr-based bulk metallic glass matrix composite. Journal of Materials Research. 2007;**22**:551

[32] Li JC, Chen XW, Huang FL. FEM analysis on the deformation and failure of fiber reinforced metallic glass matrix composite. Materials Science and Engineering A. 2016;**652**:145

[33] Zhang H, Zhang ZF, Wang ZG, Zhang HF. Deformation and damage evolution of tungsten fiber reinforced metallic glass matrix composite induced by compression. Materials Science and Engineering A. 2008;**483-484**:164

[34] Qiu KQ, Wang AW, Zhang HF, Ding BZ, Hu ZQ. Mechanical properties of tungsten fiber reinforced ZrAlNiCuSi metallic glass matrix composite. Intermetallics. 2002;**10**:1283

[35] Choi-Yim H, Johnson WL. Bulk metallic glass matrix composites. Applied Physics Letters. 1997;**71**:3808

[36] Zhang QS, Zhang W, Xie GQ, Inoue A. Unusual Plasticity of the Particulate-Reinforced Cu-Zr-Based bulk metallic glass composites. Materials Transactions. 2007;**48**:2542

[37] Conner RD, Choi-Yim H, Johnson WL. Mechanical properties of $Zr_{57}Nb_5Al_{10}Cu_{15.4}Ni_{12.6}$ metallic glass matrix particulate composites. Journal of Materials Research. 1999;**14**:3292

[38] Choi-Yim H, Conner RD, Szuecs F, Johnson WL. Processing, microstructure and properties of ductile metal particulate reinforced $Zr_{57}Nb_5Al_{10}Cu_{15.4}Ni_{12.6}$ bulk metallic glass composites Acta Materialia. 2002;**50**:2737

[39] Xu YK, Ma H, Xu J, Ma E. Mg-based bulk metallic glass composites with plasticity and gigapascal strength Acta Materialia. 2005;**53**:1857

[40] Liu T, Shen P, Qiu F, Zhang T, Jiang Q. Advanced Engineering Materials. 2009;**11**:392

[41] Chen C, Xue Y, Wang L, Cheng X, Wang F, Wang Z, Zhang H, Wang A. Microstructures and Mechanical Properties of ZrC Reinforced (Zr-Ti)-Al-Ni-Cu Glassy Composites by an In Situ Reaction. Advanced Engineering Materials. 2012;**14**:439

[42] Xue YF, Cai HN, Wang L, Wang FC, Zhang HF. Strength-improved Zr-based metallic glass/porous tungsten phase composite by hydrostatic extrusion. Applied Physics Letters. 2007;**90**:081901

[43] Pan DG, Zhang HF, Wang AM, Hu ZQ. Enhanced plasticity in Mg-based bulk metallic glass composite reinforced with ductile Nb particles. Applied Physics Letters. 2006;**89**:261904

[44] Wada T, Inoue A, Greer AL. Enhancement of room-temperature plasticity in a bulk metallic glass by finely dispersed porosity. Applied Physics Letters. 2005;**86**:251907

[45] Jang JSC, Ciou JY, Hung TH, Huang JC, Du XH. Enhanced mechanical performance of Mg metallic glass with porous Mo particles. Applied Physics Letters. 2008;**92**:011930

[46] Guo W, Wada T, Kato H. Work-hardenable Mg-based bulk metallic glass matrix composites reinforced by ex-situ porous shape-memory-alloy particles. Materials Letters. 2016;**183**:454

[47] Hays CC, Kim CP, Johnson WL. Microstructure controlled shear band pattern formation and enhanced plasticity of bulk metallic glasses containing in situ formed ductile phase dendrite dispersions. Physical Review Letters. 2000;**84**:2901

[48] Fan C, Ott RT, Hufnagel TC. Metallic glass matrix composite with precipitated ductile reinforcement. Applied Physics Letters. 2002;**81**:1020

[49] Guo W, Kato H, Yamada R, Saida J. Fabrication and mechanical properties of bulk metallic glass matrix composites by in-situ dealloying method. Journal of Alloys and Compounds. 2017;**707**:332

[50] Hofmann DC. Shape memory bulk metallic glass composites. Science. 2010;**329**:1294

[51] Xu J, Ma L, Xue Y, Nie Z, Long Y, Wang L, Deng Y. Work-hardening behavior, strain rate sensitivity, and failure behavior of in situ CuZr-based metallic glass matrix composite. Journal of Materials Science. 2016;**51**:5992

[52] Guo W, Saida J. Triple-yieldable multiphase reinforced bulk metallic glass matrix composites under tension. Materials Letters. 2017;**191**:42

[53] Hong SH, Kim JT, Lee MW, Park JM, Lee MH, Kim BS, Park JY, Seo Y, Suh JY, Yu P, Qian M, Kim KB. Combinatorial Influence of Bimodal Size of B2 TiCu Compounds on Plasticity of Ti-Cu-Ni-Zr-Sn-Si Bulk Metallic Glass Composites. Metallurgical and Materials Transactions A: Physical Metallurgy and Materials Science. 2014;**45A**:2376

[54] Hofmann DC, Suh JY, Wiest A, Lind ML, Demetriou MD, Johnson WL. Development of tough, low-density titanium-based bulk metallic glass matrix composites with tensile ductility. Proceedings of the National Academy of Sciences of the United States of America. 2008;**105**:20136

[55] Yamamoto T, Ito H, Hasegawa M, Inoue A. Mechanical properties and microstructures of composites of Ti-based metallic glass and β-Ti. Materials Transactions. 2007;**48**:1812

[56] Guo W, Kato H. Development of in-situ β-Ti reinforced Be-free Ti–based bulk metallic glass matrix composites. Journal of Alloys and Compounds. 2017;**714**:120

[57] Oka H, Guo W, Wada T, Kato H. Mg-based metallic glass matrix composite with in situ porous titanium dispersoids by dealloying in metallic melt. Materials Science and Engineering A. 2013;**582**:76

[58] Guo W, Kato H. Development and microstructure optimization of Mg-based metallic glass matrix composites with in situ B2-NiTi dispersoids. Materials and Design. 2015;**83**:238

[59] Ma H, Xu J, Ma E. Mg-based bulk metallic glass composites with plasticity and high strength. Applied Physics Letters. 2003;**83**:2793

[60] Hui X, Dong W, Chen GL, Yao KF. Formation, microstructure and properties of long-period order structure reinforced Mg-based bulk metallic glass composites. Acta Materialia. 2007;**55**:907

[61] Chen G, Zhang XL, Liu CT. High strength and plastic strain of Mg-based bulk metallic glass composite containing in situ formed intermetallic phases. Scripta Materialia. 2013;**68**:150

[62] Wang SG, Xu J. Strengthening and toughening of Mg-based bulk metallic glass via in-situ formed B2-type AgMg phase. Journal of Non-Crystalline Solids. 2013;**379**:40

[63] Zhao YY, Men H, Estévez D, Liu Y, Wang XM, Li RW, Chang CT. Mg-based bulk metallic glass composite containing in situ microsized quasicrystalline particles. Scripta Materialia. 2014;**78-79**:21